ISSN 1726-5479

SENSORS & TRANSDUCERS

vol. 139
4/12

MEMS and Modern Technologies

International Frequency Sensor Association Publishing

IFSA

Sensors & Transducers

Volume 139, Issue 4, April 2012 **www.sensorsportal.com** **ISSN 1726-5479**

Sensors & Transducers Journal (ISSN 1726-5479) is a peer review international journal published monthly online by International Frequency Sensor Association (IFSA).
Available in electronic and on CD.

Sensors & Transducers Journal

Contents

Volume 139
Issue 4
April 2012

www.sensorsportal.com

ISSN 1726-5479

Research Articles

Authors are encouraged to submit article in MS Word (doc) and Acrobat (pdf) formats by e-mail: editor@sensorsportal.com
Please visit journal's webpage with preparation instructions: http://www.sensorsportal.com/HTML/DIGEST/Submition.htm

International Frequency Sensor Association (IFSA).

Sensors & Transducers Journal, Vol. 139, Issue 4, April 2012, pp. 24-34

Sensors & Transducers

ISSN 1726-5479

http://www.sensorsportal.com

Improved Modeling of the Comb Drive Levitation Effect by Using Schwartz-Christoffel Mapping

Fengyuan LI and Jason Vaughn CLARK
Purdue University, 1205 W. State St., West Lafayette, IN, 47906, USA
Tel.: +1-765-494-3437, fax: +1-765-494-2806
E-mail: li200@purdue.edu, jvclark@purdue.edu

Received: 7 December 2011 /Accepted: 23 April 2012 /Published: 30 April 2012

Abstract: In this paper we model the comb drive levitation effect quickly and accurately by using Schwarz-Christoffel mapping (SCM) and study the sensitivity of the levitation effect to the comb finger width and the gap between the comb fingers. The levitation effect occurs when the substrate is within close proximity to the comb fingers. Lumped comb drive models found in the literature ignore the levitation effect, which decreases their accuracy. Previously, potential theory method, finite element analysis (FEA) and boundary element analysis (BEA) were used to model the levitation effect. We show that the levitation effect can be modeled more quickly and accurately by using SCM in this paper. Our method is several times faster than FEA because it does not discretize the boundaries or subdomains into a large number of coupled equations. We find that the vertical forces on a rotor finger are in balance when the levitation is 1.239 ± 0.001 μm for 4 μm wide, $2\mu m$ thick comb fingers with 2 μm gap apart from each other and apart from the substrate. This result is slightly larger and more accurate than previously reported values. Our improvement in accuracy is most likely because our model includes all the electric fields around the rotor finger, captures the effect of the periodic array of comb fingers, treats the electrostatic fields at the vertices exactly, and uniquely considers reflection due to a multitude of neighboring comb drive fingers. *Copyright © 2012 IFSA.*

Keywords: Comb drive, Levitation, Modeling and simulation, Online tool, Schwarz-Christoffel mapping.

1. Introduction

Comb drives have been widely used in the field of microelectromechanical systems (MEMS) since its invention in 1980's [1]. They have been playing important roles in many applications such as resonators [2], accelerometers [3], gyroscopes [4], micro-manipulators [5], and material property test beds [6]. A comb drive typically consists of a stator anchored to a substrate and a moveable rotor attached to supporting flexures. The stator and rotor are electrically coupled with moveable interdigitated electrodes (comb drive fingers). See Fig. 1 [2]. The comb drive is usually used as a deflection sensor via capacitance or an actuator via an electrostatic force.

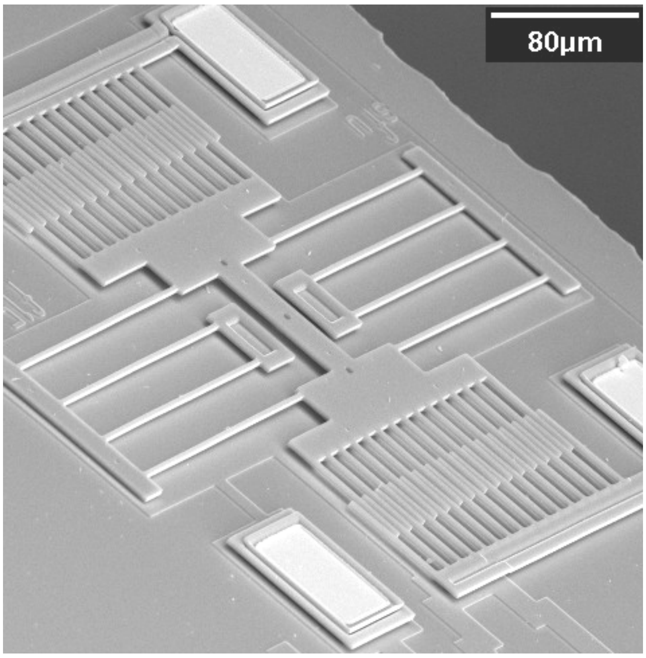

Fig. 1. Comb drive folded flexure. This microdevice consists of two symmetric folded flexures coupled to a pair of comb drives. A voltage applied across a comb drive generates an electrostatic force to cause the in-plane deflection. However, due to charge asymmetry about the comb fingers, the comb drive also experiences a small out-of-plane deflection. Another effect of charge asymmetry can be seen in the scanning electron image, where the back bone of the structure produces a larger shadow than the shadow of the adjacent anchors. This particular out-of-plane deflection is due to the device being charged by a scanning beam of electrons while under inspection.

Most of the aforementioned applications take advantage of the in-plane displacement of the rotor. The in-plane displacement is caused by the electrostatic force when there is a potential difference between the interdigitated fingers on the rotor and stator. Compared to other important electrostatic actuation configurations, such as parallel-plate configuration, comb drive provides relatively large in-plane displacement because of its relatively large stable region.

However, out-of-plane displacement of the rotor, known as the comb drive levitation effect [7], could occur. The levitation effect is caused by an asymmetric electric field about the rotor fingers when the substrate is within close proximity to the comb fingers. If the substrate is at the same potential as the rotor fingers, then the surface charge density on the surfaces of the rotor fingers that are nearest to the substrate is lower than the surface charge density on the surfaces that are furthest away from the substrate. Static surface charge on a conductor produces a surface pressure that is outward and normal to the surface. This surface pressure is proportional to the surface charge density squared [8]. Hence, the greater the surface charge, the greater the surface pressure. Therefore, the net surface pressure about the rotor fingers directs away from the substrate, which forces the rotor fingers away from the substrate.

The levitation effect can be substantial for MEMS having out-of-plane stiffness on the same order as in-plane stiffness. The levitation effect is undesirable in many applications. In [9], the levitation effect caused the micromotor scanner performance to degrade as the rotor tilted out of the rotational plane producing sporadic rotation. The operating voltage of the scanner was limited to reduce the levitation effect. In [10], the levitation effect caused more than 50 % reduction in scale factor and more than 0.1 % increase in cross-axis sensitivity of a typical surface micromachined gyroscope. It was concluded that the levitation effect should not be ignored in high grade gyroscope designs. And in [11], the levitation effect caused the misalignment between the beam and the post during the sidewall friction and wear tests. The misalignment was ignored when finding the contact area. Several methods have been proposed to eliminate or reduce the levitation effect. In [7], new electrode configurations and electrical routing schemes were proposed so as to reduce the levitation effect. In [12], the substrate underneath the fingers was removed by etching to promote a symmetric electric field about the rotor fingers to eliminate the levitation effect. However, these methods increase the fabrication complexity and increase comb drive size.

On the other hand, the levitation effect has also been taken advantage of in some other applications. In [13], the levitation effect was used to design vertical-to-the-substrate actuation for optical phase shifting interferometry applications. In [14], the levitation effect was used to investigate the static friction effect between polysilicon surfaces. And in [15], the levitation effect was used to excite both the bending and torsion vibration modes of a comb drive resonant strain gauge.

In order to better understand the comb drive levitation effect, several modeling methods have been proposed. In [16], potential theory method was used to derive the analytical levitation model; however, the electric field emanating from the lower surface of the rotor finger was ignored. In [7] and [17], FEA-based software and BEA were used, respectively; however, both methods often require large computational memory and time because they need to discretize the subdomains or boundaries into a large number of coupled equations. The accuracy of these methods relies on the meshing refinement. And they are not able to treat the electrostatic fields at the vertices exactly, which deteriorates the accuracy. For the same comb drive design (4 μm wide, 2 μm thick comb fingers with 2 μm gaps apart from each other and apart from the substrate), the levitation found in [7] and [17] was 1.22 μm and 1.19 μm, respectively, when the vertical forces on the rotor fingers are in balance. The results are 2.5 % different.

In our prior effort [18], we developed an online tool based on the SCM at nanoHUB.org through a web interface and remote computation. In this paper, we review the SCM-based algorithm of our tool, provide detailed verification, and investigate the sensitivity of the levitation effect to the comb drive design parameters.

The rest of this paper is organized as follows. In Section 2 we review the algorithm of our tool. In Section 3 we present, compare, and verify our results. In Section 4, we investigate the sensitivity of the levitation effect to two comb drive design parameters. And in Section 5 we summarize what we learn from this effort.

2. Algorithm

In this section, we review the SCM-based algorithm presented in [18]. The comb drive configuration under investigation is shown in Fig. 2 (a). It consists of an array of interdigitated fingers. Fig. 2 (b) shows a cross section of a part of the array, showing a levitated rotor finger with the levitation, z. The domain of one pair of fingers is identified by dashed lines in Fig. 2 (b). In Fig. 2 (c), we show our SCM configuration. We capture the effect of the periodic array in the model by reflecting the image of the domain to both the left and the right directions. The boundaries of the substrate and the rotor finger are grounded, and the boundaries of the stator finger have a constant potential, *V*. That is, they have Dirichlet boundary conditions. The reflective boundaries have Neumann boundary conditions, i.e. $\partial V / \partial y = 0$. We assume that all structures are perfect conductors, have perfect vertices, and have flat sidewalls.

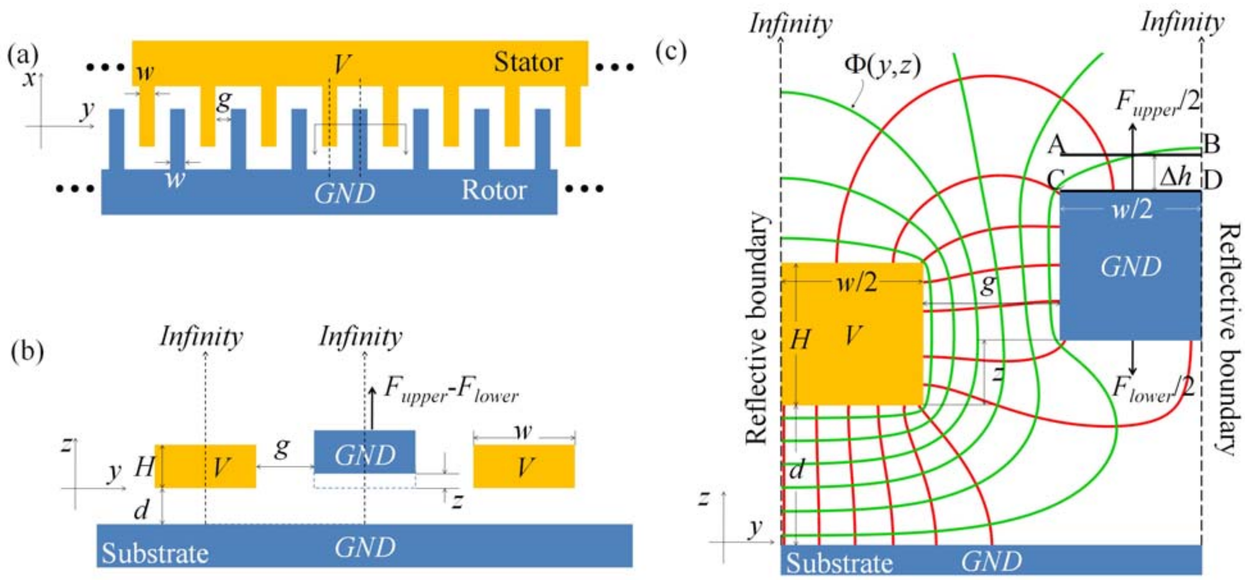

Fig. 2. Comb finger configuration. In (a)-(c), the stators have a surface potential, *V*, and the rotors and substrates are grounded, denoted as GND. (a) We show an overhead view of a comb drive with a large number of comb fingers of width, w, and gap, g. We consider a subset of the periodic array of comb fingers that captures the contributions of the large number other fingers through reflective boundaries. (b) We show the levitation of the rotor, z, its net electrostatic force, and the substrate. The electrostatic force consists of a net distributed force normal to the upper and lower boundaries of the rotor F_{upper} and F_{lower}. (c) The vertical dashed lines are reflective Neumann boundaries and the substrate and the boundaries of the fingers are Dirichlet boundaries. The quantities H and d are the layer thickness and initial gap between the finger and substrate. The electric field is shown as red field lines perpendicular to surfaces, and the equipotential lines are shown as green field lines parallel to surfaces. The potential distribution along the segment AB, a small distance Δh above the rotor finger, is used to find the electrostatic pressure along the upper boundary of the rotor finger by (1)-(3). The size of Δh is exaggerated for better illustration purpose.

We use a MATLAB-based numerical SCM tool [19] to model the domain shown in Fig. 2 (c) as a simply connected polygon. The potential distribution, $\Phi(y,z)$, within the domain can be obtained. The electric field $\mathbf{E}(y,z)$ is equal to the negative gradient of the potential distribution [8],

$$\mathbf{E}(y,z) = -\nabla\Phi(y,z). \tag{1}$$

We use bold letters to represent vectors in this paper.

We use Newton's difference quotient to find the electric field component in *z*-direction, $\mathbf{E}_z(y)$, along the upper and lower boundaries of the rotor finger numerically,

$$\mathbf{E}_z(y) = -\frac{\Phi(y, z+\Delta h) - \Phi(y,z)}{\Delta h}, \tag{2}$$

where Δh is the distance between the upper boundary of the rotor finger and the segment *AB*. Since we assume that the material of both the rotor and the stator is conductors, the electrostatic pressure component in *z*-direction can be calculated as [8]

$$P_z(y) = \frac{\varepsilon_0 \left|\mathbf{E}_z\left(y\right)\right|^2}{2}, \tag{3}$$

where ε_0 is the permittivity of free space. The magnitude of the electrostatic forces per unit depth along the boundaries of the rotor finger, F_{upper} and F_{lower}, can be calculated as

$$F_z(y_0) = P_z(y_0)dy, \tag{4}$$

where dy is the length of the small interval containing the point y_0.

The algorithm is summarized in Fig. 3. We repeat the process for the rotor finger with different levitations in order to find the value, z_0, where the vertical electrostatic forces on the upper and lower boundaries of the rotor finger, F_{upper} and F_{lower}, are in balance.

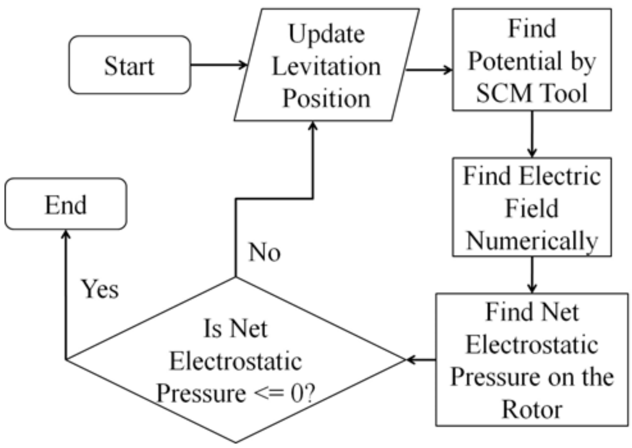

Fig. 3. The flow chart of our SCM algorithm.

3. Result and Verification

In this section, we find the potential distribution, $\Phi(y,z)$, within the domain of interest using the numerical SCM tool and verify it by using an FEA-based software, COMSOL 3.5 a. Once the potential distribution is found and verified. We follow the algorithm presented in Section 2 to find the levitation where the vertical electrostatic forces on the rotor finger are in balance. That is, the net vertical electrostatic pressure on the rotor finger is zero. In order to compare our results to the ones of FEA and BEA, we use the comb fingers with the same geometric dimensions as those in [7] and [17]. That is, the width, w, and the thickness, H, of the comb fingers are 4 μm and 2 μm, respectively. The air gap, g, between the stator and the rotor fingers is 2 μm. And the initial air gap, d, between the fingers and the substrate is 2 μm.

3.1. Potential Distribution

The potential distribution is found with the numerical SCM tool by solving the Laplace's equation on the simply connected polygonal domain, subject to piecewise constant Dirichlet and homogeneous Neumann boundary conditions [19]. To verify the potential distribution found by the numerical SCM tool, we compare our results with the results in COMSOL 3.5 a. The domain under investigation in COMSOL 3.5 a is shown in Fig. 4 (a). The potential distribution found with initial mesh is color-mapped. Note that the horizontal scale is 2.5 times larger than the vertical scale for better illustration purpose in Fig. 4 (a)-(c). The stator boundaries are at 20 V. The rotor boundaries and the substrate (red dash line) are grounded. And the rest boundaries of the air box (yellow dash lines) are set as zero charge/symmetry boundary conditions. That is, the potential distribution is symmetric with respect to these boundaries. Note that the upper boundary of the air box goes to infinity in the SCM, while the air box in COMSOL 3.5 a model has a finite size here. In order to reduce the effect of the size of the air box, we set the height of the air box as 20 μm, 10 times as large as the thickness of the comb fingers. The levitation of the rotor finger shown in Fig. 4(a) is 1 μm.

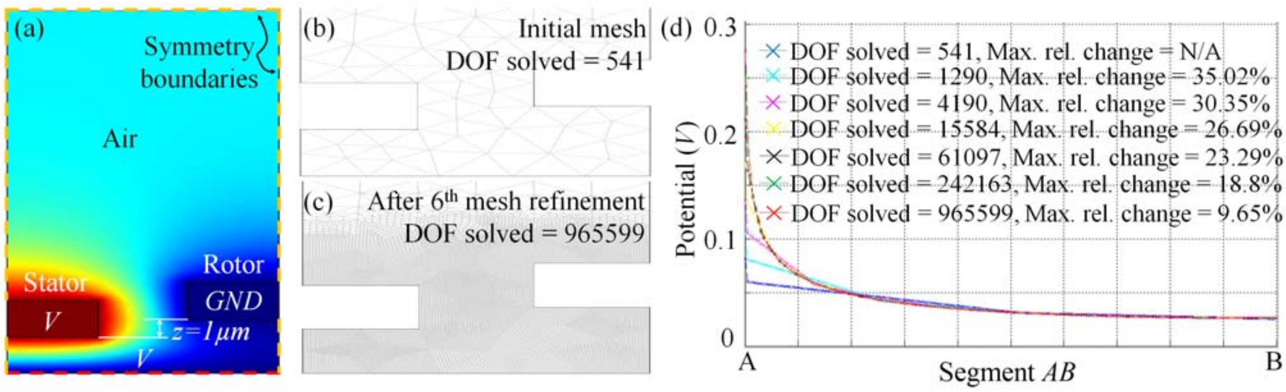

Fig. 4. Potential distribution convergence analysis using FEA. Note that the horizontal scale is 2.5 times larger than the vertical scale for better illustration purpose in (a)-(c). (a) The domain simulated in COMSOL 3.5a FEA is shown with color-mapped potential distribution. The width w and the thickness H of the fingers are 4 μm and 2 μm, respectively. The air gap g between the stator and the rotor fingers is 2 μm. And the air gap d between the rotor finger and the substrate is 3 μm with 1 μm levitation. The boundaries of the stator finger are 20 V. The boundaries of the rotor finger and the substrate (red dash line) are grounded. The rest boundaries of the air box (yellow dash lines) are set as zero charge/symmetry boundary conditions. That is, the potential symmetric with respect to these boundaries. (b) We show the initial mesh quality around the finger area with the free mesh option in COMSOL 3.5a. (c) We show the mesh quality after six mesh refinements around the same finger area in COMSOL 3.5a. (d) The mesh convergence analysis result is shown. The solved DOF and the maximum relative change of potential after each mesh refinement are given. Due to our 4 GB RAM limitation, our maximum mesh refinement was only able to decrease the relative change to 9.65 % using FEA.

We perform the mesh convergence analysis as shown in Fig. 4 (b)-(d). We use the free mesh option with triangular mesh elements in COMSOL 3.5a. The potential along the segment AB which is shown in Fig. 2 (c) is evaluated. We choose the distance between the segment AB and the upper boundary of the rotor finger to be Δh = 0.01 4 μm. We choose the interval between each evaluation point along the segment AB as 0.01μm. In Fig. 4 (b) and (c), we show the initial mesh quality and the mesh quality after six mesh refinements around the finger area. In Fig. 4(d), we compare the potential along the segment AB with increasing time of mesh refinement. The maximum relative change of potential is defined as the maximum of the ratio of the potential difference at each evaluation point with current mesh condition to the potential at the same evaluation point with the previous mesh condition. Therefore, the maximum relative change with the first mesh condition is not defined, shown as N/A in

Fig. 4(d). We stop the mesh refinement until the maximum relative change decreases to 9.65 %. The simulation of the model with further mesh refinement requires more than 4GB computer memory.

We compare the potential along segment AB found by SCM to the results in COMSOL 3.5 a with six mesh refinements in Fig. 5. The maximum relative difference is 1.69 % if we ignore the potential fluctuations identified with the black circle in Fig. 5. We find that the potential fluctuations happen when segment AB is close enough to the rotor finger. For example, the potential distribution is smooth when Δh is 0.1 μm instead of 0.01 μm. We think the undesired fluctuations are caused by the numerical instability in the numerical SCM tool, but further investigations are needed. For an FEA convergence of 9.65 %, our SCM method is over 3 times faster. We were not able to compare speeds to better than 9.65 % FEA convergence due to the large FEA memory requirements and the 4GB memory limitation of our computer.

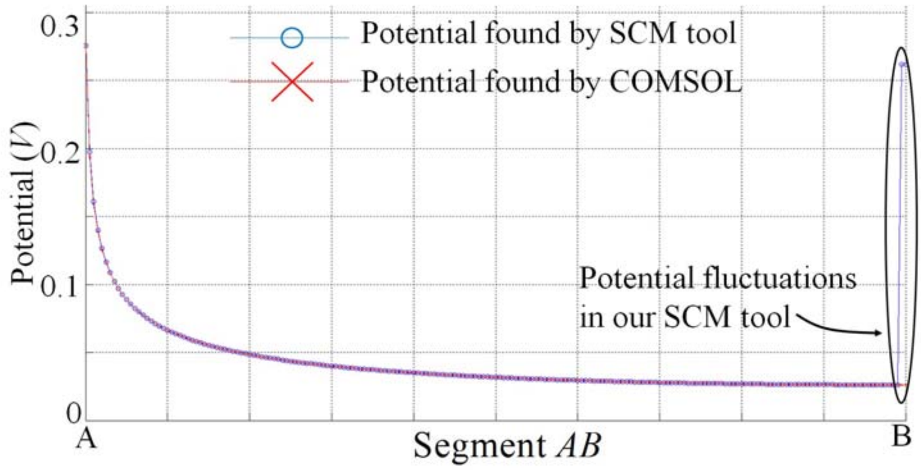

Fig. 5. Verification of the potential distribution. We compare the potential distribution along the segment AB found by SCM against the results found in COMSOL 3.5a with the six mesh refinements shown in Fig. 4(c). We find that the potential fluctuations happen when the segment AB is close enough to the rotor finger. The maximum relative difference is 1.69 % if we ignore the potential fluctuations noted with the black circle.

3.2 Electric Field and Electrostatic Pressure

Once we find the potential distribution, (2) and (3) are used to find the electric field and the electrostatic pressure along the upper and lower boundaries of the rotor finger. We set the step size Δh as 0.1 μm where the SCM potential fluctuates to avoid numerical instability, and as 0.01 μm elsewhere along the boundaries. The electric field and the electrostatic pressure along the upper boundary of the rotor finger found by our tool are compared against COMSOL 3.5a results in Fig. 6(a) and (b), respectively. The maximum relative differences between the results found by two methods are 1.69 % for the electric field and 3.4 % for the pressure. And the results are smooth along the entire boundary after choosing larger step size for the positions where the potential fluctuates.

3.3. Levitation

We plot the electrostatic force per unit depth of the rotor finger with respect to different levitation for three applied voltages in Fig. 7. The levitation is 1.239 ± 0.001 μm when the vertical forces on the rotor finger are in balance. That is, the electrostatic force per unit depth is 0 nN/ μm on the rotor finger. Note that we assume that the rotor does not connect any flexures providing vertical mechanical restoring force. We evaluate the electrostatic force per unit depth of the rotor finger with the levitation step size of 0.01 μm. That is why the uncertainty for the result presented here is 0.001 μm. More precise result can be found by reducing the levitation step size, however, more computational cost is expected. Fig. 7 shows that the levitation we found is independent of the applied voltage. And the electrostatic force per unit depth on the rotor decreases linearly with the increase of the levitation. Our result is larger than those reported previously, 1.22 μm in [7] by FEA and 1.19 μm in [17] by BEM. This is possibly because our SCM configuration captures the levitation contributions due to the multitude of other fingers in the comb finger array and due to a more accurate and precise electrostatic pressure at the corner edges.

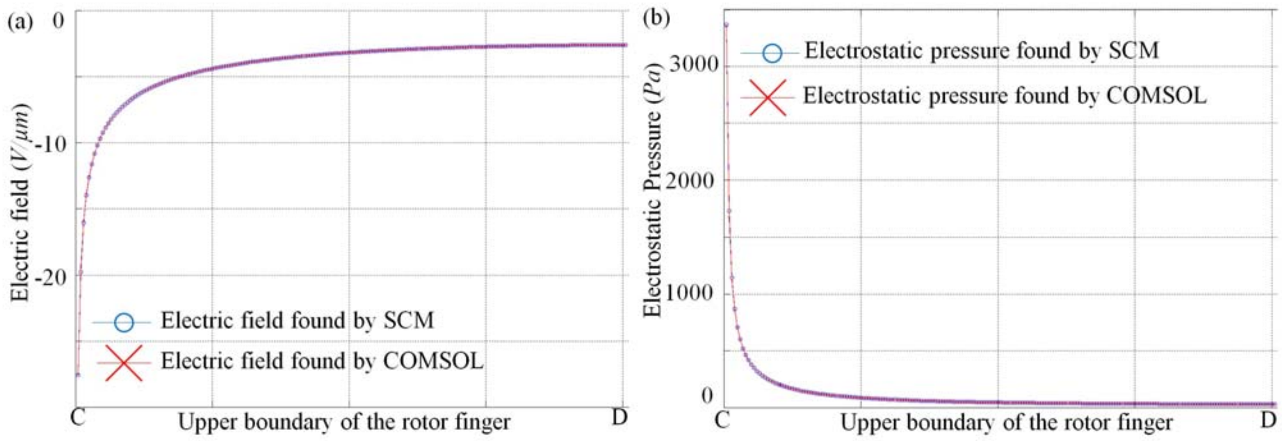

Fig. 6. Electric field and electrostatic pressure along the upper boundary of the rotor finger shown in Fig. 2 (c). (a) We compare the electric field against the COMSOL results, and the relative error is 1.69 %. The negative value means the electric fields point in the negative *z*-direction. (b) We compare the electrostatic pressure against the COMSOL results, and the relative error is 3.4 %.

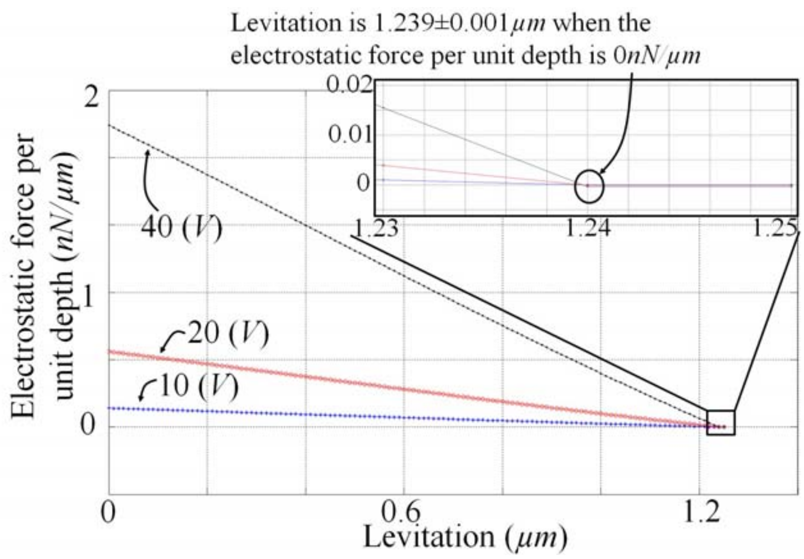

Fig. 7. Electrostatic force per unit length of the rotor finger vs. levitation. The levitation is 1.239 ± 0.001 μm when the vertical forces on the rotor finger are in balance. This levitation result is independent of the applied voltage.

4. Sensitivity Analysis

In this section, we use our tool to investigate the sensitivity of the comb drive levitation effect to two comb drive design parameters. We find the levitation where the vertical forces on the rotor are in balance while sweep the width of the comb fingers, w, and the gap between two adjacent comb fingers, g. We choose these two parameters because the in-plane parameters can be easily adjusted in layout design. That is, the out-of-plane parameters such as the thickness of the comb fingers, H, and the gap between the comb fingers and the substrate, d, cannot be changed as easily as the in-plane ones in layout design.

In Fig. 8, we show the levitation of the rotor finger with the change of the finger widths and the gap between adjacent comb fingers. The other geometries remain the same as the model described in Section 3. The vertical forces on the rotor finger are in balance at the levitation we find. We find that the levitation is about linearly proportional to the increase of both design parameters. We use the 1st-order polynomial to fit the data as shown by the red dash lines in Fig. 8. We define the slope of the 1st-order polynomial fit as the sensitivity of the levitation effect to the corresponding design parameter. The sensitivities of the levitation effect to the finger width, w, and the gap between adjacent comb fingers, g, are about 0.058 and 0.892, respectively.

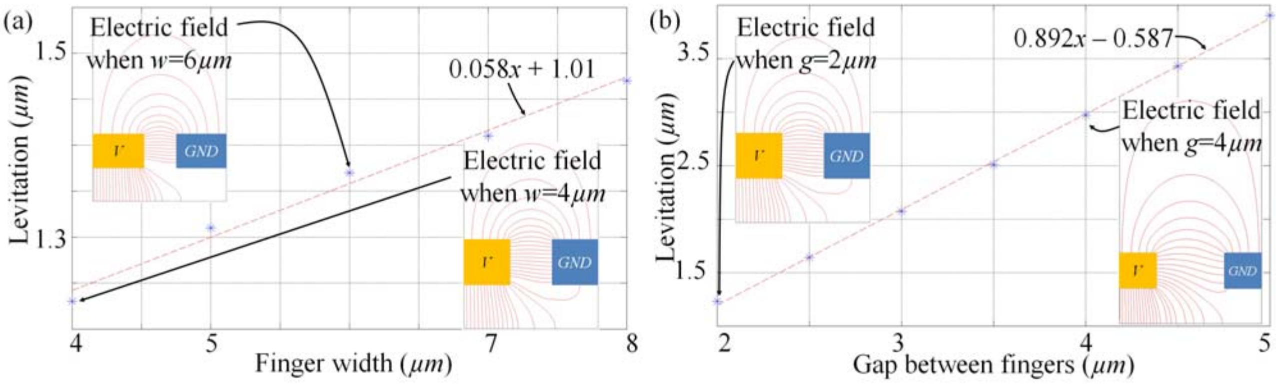

Fig. 8. Sensitivity analysis of the levitation effect to two design parameters. The vertical forces on the rotor are in balance at the levitation we find. We use the 1st-order polynomial to fit the data as shown by the red dash lines. We define the slope of the 1st-order polynomial fit as the sensitivity of the levitation effect to the corresponding design parameter. (a) Levitation VS. Finger width; (b) Levitation vs. Gap between fingers. We find that the levitation is about linearly proportional to the increase of both design parameters. The sensitivities of the levitation effect to the finger width and the gap between adjacent comb fingers are about 0.058 and 0.892, respectively.

With the increase of the finger width while keeping the other geometric parameters unchanged, the electric field around the rotor finger becomes more asymmetric. That is, the electric field lines become more difficult to reach the lower boundary of the rotor finger while they can reach its upper boundary as easily as before. Two insets in Fig. 8 (a) show the electric field plotted by COMSOL 3.5 a streamline plot when the finger width is 4 μm and 6 μm. We apply 20 V on the stator finger (yellow) and ground the rotor finger (blue). We use the Magnitude Controlled option with density value set as 12 when plotting the electric fields in both insets for qualitative comparison. By using Magnitude Controlled option, the plotted field lines accord to the magnitude of the electric field. As we can see that the electric field lines are denser underneath the rotor finger when w=4 μm. Note that the density of the electric field lines indicates the density of the charge distribution. And the electrostatic surface pressure is proportional to the surface charge density squared as mentioned in Section 1. Thus we can expect that the initial electrostatic surface pressure on the rotor finger becomes larger with the increase of the comb finger widths. Therefore, the rotor finger needs to levitate more so as to balance the electrostatic surface pressure vertically.

Similarly, with the increase of the gap between fingers while keeping the other geometric parameters unchanged, the electric field around the rotor finger becomes more asymmetric as well as shown by two insets in Fig. 8 (b) qualitatively. Both insets are created by using the same method as the one mentioned above. The electric field lines are less dense along the lower boundary of the rotor finger because the rotor finger is relatively far away from the stator finger when the distance to the substrate remains the same. However, the electric field density on the upper boundary of the rotor finger should be less affected with this distance change. Therefore, the levitation of the rotor finger is expected to increase with the increase of the gap between fingers.

5. Summary

In this paper, we presented the algorithm of our online tool that can model the comb drive levitation effect more quickly and accurately than previous efforts using finite element analysis (FEA). We compared our results to the ones reported previously and verified our results by comparing them to the ones found by FEA with convergence analysis. And we used our tool to find the sensitivity of the levitation effect to two comb drive design parameters: the width of the comb fingers and the gap between two adjacent comb fingers. Our SCM method is more computationally efficient and accurate compared to conventional methods. We found that the levitation is 1.239 ± 0,001 μm for 4 μm wide, 2 μm thick, comb fingers separated from each other and the substrate by 2 μm gaps. Our value is 1-10 % larger than the values reported previously (1.19 μm and 1.22 μm). We think this is because our SCM configuration captures the levitation contributions due to the multitude of other fingers in the comb finger array and accurately accounts for the fringing field charges at the corners of the geometry. Compared to the time FEA takes to compute with 9.65% convergence, our SCM method is over 3 times faster. We studied the sensitivity of the levitation effect to the comb finger width and the gap between adjacent comb fingers. In both cases, the levitation increases with the increase of these two design parameters, while the levitation effect is more sensitive to the gap between fingers. Future research directions might include curved edges, course sidewalls, and the development of a lumped element model for this comb drive levitation effect.

Acknowledgements

The authors would like to acknowledge Prof. Driscoll at University of Delaware for insightful discuss on the MATLAB-based numerical SCM tool. This work was supported by the National Science Foundation Cyber-Enabled Discovery and Innovation and the nanoHUB.

References

[1]. W. C. Tang, T-C. H. Nguyen, R. T. Howe. Laterally driven polysilicon resonant microstructures, *Sensors and Actuators*, Vol. 20, 1989, pp. 25–32.

[2]. W. C. Tang, T-C. H. Nguyen, M. W. Judy, R. T. Howe. Electrostatic-comb drive of lateral polysilicon resonators, *Sensors and Actuators*, Vol. 21, 1990, pp. 328-331.

[3]. S. D. Senturia, Microsystem Design, 1st ed., *Springer*, 2000.

[4]. C. Acar, A. Shkel, MEMS Vibratory Gyroscopes: Structural Approaches to Improve Robustness, 2nd ed., *Springer*, 2008.

[5]. B. R. D. Jong, D. M. Brouwer, M. J. D. Boer, H. V. Jansen, H. M. J. R. Soemers, G. J. M. Krijnen, Design and fabrication of a planar three-DOFs MEMS-based manipulator, *Journal of Microelectromechanical Systems*, Vol. 19, 2010, pp. 1116-1130.

[6]. D. Zhang, J. Breguet, R. Clavel, V. Sivakov, S. Christiansen, J. Michler, In situ electron microscopy mechanical testing of silicon nanowires using electrostatically actuated tensile stages, *Journal of Microelectromechanical Systems*, Vol. 19, 2010, pp. 663-674.

[7]. W. C. Tang, M. G. Lim, R. T. Howe, Electrostatic comb drive levitation and control method. *Journal of Microelectromechanical Systems*, Vol. 1, 1992, pp. 170-178.

[8]. D. J. Griffiths, Introduction to Electrodynamics, 3rd ed., *Addison Wesley*, 1999.

[9]. A. A. Yasseen, J. N. Mitchell, D. A. Smith, M. Mehregany, High-aspect-ratio rotary polygon micromotor scanners. *Sensors and Actuators A: Physical*, Vol. 77, 1999, pp. 73-79.

[10]. C. Painter, A. Shkel, Effect of levitation forces on the performance of surface micromachined MEMS gyroscopes, *Proc. of IEEE Sensors*, 2004, pp. 508-511.

[11]. D. H. Alsem, R. Van der Hulst, E. A. Stach, M. T. Dugger, J. T. M. De Hosson, R. O. Ritchie, Wear mechanisms and friction parameters for sliding wear of micron-scale polysilicon sidewalls, *Sensors and Actuators A: Physical*, Vol. 163, 2010, pp. 373-382.

[12]. F. Li, J. V. Clark, Practical measurements of stiffness, displacement, and comb drive force of MEMS, *18th Biennial University/Government/Industry Micro/Nano Symp*, 2010.

[13]. A. P. Lee, C. F. McConaghy, G. Sommargren, P. Krulevitch, E. W. Campbell, Vertical-actuated electrostatic comb drive with in situ capacitive position correction for application in phase shifting diffraction interferometry, *Journal of Microelectromechanical Systems*, Vol. 12, 2003, pp. 960-971.

[14]. A. Lumbantobing, K. Komvopoulos, Static friction in polysilicon surface micromachines, *Journal of Microelectromechanical Systems*, Vol. 14, 2005, pp. 651-663.

[15]. R. G. Azevedo, W. Huang, O. M. O'Reilly, A. P. Pisano, Dual-mode temperature compensation for a comb-driven MEMS resonant strain gauge, *Sensors and Actuators A: Physical*, Vol. 144, 2008, pp. 374-380.

[16]. H. Hammer, Analytical model for comb-capacitance fringe fields, *Journal of Microelectromechanical Systems*, Vol. 19, 2010, pp. 175-182.

[17]. S. W. Chyuan, Y. S. Liao, J. T. Chen, Computational study of the effect of finger width and aspect ratios for the electrostatic levitating force of MEMS combdrive, *Journal of Microelectromechanical Systems*, Vol. 14, 2005, pp. 305-312.

[18]. F. Li, J. V. Clark, Improved modeling of the comb drive levitation effect, *Nanotechnology Conf. and Expo.*, 2010.

[19]. T. A. Driscoll, L. N. Trefethen, Schwarz-Christoffel Mapping, *Cambridge University Press*, 2002.

Guide for Contributors

Aims and Scope

Sensors & Transducers Journal (ISSN 1726-5479) provides an advanced forum for the science and technology of physical, chemical sensors and biosensors. It publishes state-of-the-art reviews, regular research and application specific papers, short notes, letters to Editor and sensors related books reviews as well as academic, practical and commercial information of interest to its readership. Because of it is a peer reviewed international journal, papers rapidly published in *Sensors & Transducers Journal* will receive a very high publicity. The journal is published monthly as twelve issues per year by International Frequency Sensor Association (IFSA). In additional, some special sponsored and conference issues published annually. *Sensors & Transducers Journal* is indexed and abstracted very quickly by Chemical Abstracts, IndexCopernicus Journals Master List, Open J-Gate, Google Scholar, etc. Since 2011 the journal is covered and indexed (including a Scopus, Embase, Engineering Village and Reaxys) in Elsevier products.

Topics Covered

Contributions are invited on all aspects of research, development and application of the science and technology of sensors, transducers and sensor instrumentations. Topics include, but are not restricted to:

- Physical, chemical and biosensors;
- Digital, frequency, period, duty-cycle, time interval, PWM, pulse number output sensors and transducers;
- Theory, principles, effects, design, standardization and modeling;
- Smart sensors and systems;
- Sensor instrumentation;
- Virtual instruments;
- Sensors interfaces, buses and networks;
- Signal processing;
- Frequency (period, duty-cycle)-to-digital converters, ADC;
- Technologies and materials;
- Nanosensors;
- Microsystems;
- Applications.

Submission of papers

Articles should be written in English. Authors are invited to submit by e-mail editor@sensorsportal.com 8-14 pages article (including abstract, illustrations (color or grayscale), photos and references) in both: MS Word (doc) and Acrobat (pdf) formats. Detailed preparation instructions, paper example and template of manuscript are available from the journal's webpage: http://www.sensorsportal.com/HTML/DIGEST/Submition.htm Authors must follow the instructions strictly when submitting their manuscripts.

Advertising Information

Advertising orders and enquires may be sent to sales@sensorsportal.com Please download also our media kit: http://www.sensorsportal.com/DOWNLOADS/Media_Kit_2012.pdf